Journal of Computational Physics 368 (2018) 196–209

Contents lists available at ScienceDirect

Journal of Computational Physics

www.elsevier.com/locate/jcp

Gaussian basis implementation of the charge patching method

Zarko Bodroski [a], Nenad Vukmirović [b,*], Srdjan Skrbic [a,*]

[a] University of Novi Sad, Faculty of Sciences, Department of Mathematics and Informatics, Trg Dositeja Obradovica 4, 21000 Novi Sad, Serbia
[b] Scientific Computing Laboratory, Center for the Study of Complex Systems, Institute of Physics Belgrade, University of Belgrade, Pregrevica 118, 11080 Belgrade, Serbia

ARTICLE INFO

Article history:
Received 6 October 2017
Received in revised form 5 April 2018
Accepted 17 April 2018
Available online 22 April 2018

Keywords:
Charge patching method
Density functional theory
Gaussian basis
Electronic structure
Semiconductors

ABSTRACT

We present the implementation of the density functional theory based charge patching method using the basis of Gaussian functions. The method is based on the assumption that the electronic charge density of a large system is the sum of contributions of individual atoms, so called charge density motifs, that are obtained from calculations of small prototype systems. In our implementation wave functions and electronic charge density are represented using the basis of Gaussian functions, while charge density motifs are represented using a real space grid. A constrained minimization procedure is used to obtain Gaussian basis representation of charge density from real space representation of motifs. The code based on this implementation exhibits superior performance in comparison to previous implementation of the charge patching method using the basis of plane waves. It enables calculations of electronic structure of systems with around 1000 atoms on a single CPU core with computational time of just several hours.

1. Introduction

Density functional theory (DFT) [1–3] is arguably the most useful approach for electronic structure calculations of physical systems containing a large number of atoms. There is currently a variety of computational codes that implement DFT equations in the basis set of plane waves [4–7], Gaussians [8,9], localized numerical orbitals [10], using real-space representation [11,12], as well as using other approaches [13]. Nevertheless, there is a huge interest to make further progress in the development of methods for electronic structure calculations. In that regard, several different and complementary research directions are currently pursued worldwide. One direction is devoted to develop methods that give accurate results in cases where standard approximations in DFT are known to fail – these developments include many body theory in GW approximation [14] (where G stands for Green's function and W for screened Coulomb interaction), the development of new density functionals [15,16] or methods specialized for strongly correlated materials such as dynamical mean field theory [17]. A second important direction includes the development of more efficient numerical schemes that enable calculations of larger systems and efficient exploitation of high performance computing facilities [18–24]. A third equally important direction is based on exploiting certain well grounded approximations in DFT that significantly speed up DFT calculations and open the way for analysis of rather large systems. The methods developed along this line include the density functional tight-binding method [25,26], the fragment molecular orbital method [27], the semiempirical pseudopotential method [28,29], the charge patching method (CPM) [30–32], the exchange-correlation potential patching method [33], etc.

* Corresponding authors.
E-mail addresses: zarko.bodroski@dmi.uns.ac.rs (Z. Bodroski), nenad.vukmirovic@ipb.ac.rs (N. Vukmirović), srdjan.skrbic@dmi.uns.ac.rs (S. Skrbic).

https://doi.org/10.1016/j.jcp.2018.04.032
0021-9991/

Central idea of the last three methods is to directly construct the single-particle Kohn–Sham Hamiltonian without doing self-consistent DFT calculations. Each of these methods is based on the assumption that a certain relevant quantity can be decomposed into contributions of individual atoms. These contributions are extracted from calculations on small prototype systems and the relevant quantity for a large system is calculated simply by adding contributions of individual atoms. In the case of pseudopotential method, the relevant quantity is the single-particle potential, in the case of exchange-correlation patching method, the relevant quantity is the exchange-correlation potential, while in the case of charge patching method, it is the electronic charge density.

Existing implementation of the charge patching method uses the basis of plane waves to represent the wave functions [32]. While plane-wave basis offers several advantages, such as ease of implementation of relevant equations and the ability to systematically truncate the basis based on kinetic energy cut-off, it has a drawback that quite a large number of plane waves is necessary to accurately describe the wave functions in the neighborhood of an atom. On the other hand, the basis sets containing localized Gaussian functions, developed in the quantum chemistry community [8,9], offer advantage that wave functions can be represented with a small number of Gaussians. While there is no simple systematic way to truncate the basis set, one can exploit some of widely used and tested basis sets obtained after more than half a century of development.

In this work, we present the implementation of the charge patching method in the basis of Gaussian functions. Such an implementation offers a large speed-up in comparison to previous plane wave implementation. The paper is organized as follows. In Sec. 2 we review the charge patching method. In Sec. 3 we present the details of our implementation of CPM in the basis of Gaussian functions with a particular emphasis on the parts of implementation that are not present in the implementation of DFT in Gaussian basis. In Sec. 4 we present the performance of the serial code and demonstrate that one can calculate the systems with around 1000 atoms on a single CPU core with computational times of just several hours. We also demonstrate for several different classes of systems that our CPM implementation in Gaussian basis yields electronic states with accuracy similar as DFT implementation in the same basis.

2. Description of the charge patching method

In standard DFT calculations, one has to self-consistently solve the Kohn–Sham equations [2]

$$\left(-\frac{\hbar^2}{2m_0}\nabla^2 + V_{ion} + V_H[\rho] + V_{xc}[\rho]\right)\psi_i(\mathbf{r}) = \varepsilon_i\psi_i(\mathbf{r}) \tag{1}$$

and the equation that relates the electronic charge density $\rho(\mathbf{r})$ and the single-particle wave functions $\psi_i(\mathbf{r})$ that reads:

$$\rho(\mathbf{r}) = -|e|\sum_i |\psi_i(\mathbf{r})|^2 . \tag{2}$$

In previous equations m_0 is the free electron mass, $\hbar$ is the reduced Planck's constant, e is the elementary charge, V_{ion} is the potential of nuclei and core electrons, $V_H[\rho]$ is the electrostatic (Hartree) potential of the valence electronic charge density $\rho(\mathbf{r})$, $V_{xc}[\rho]$ is the exchange-correlation potential which, under the local density approximation (LDA), depends only on the electronic charge density at a given point in space, while ε_i is the eigenenergy of a single-particle state i. The summation in Eq. (2) includes all occupied electronic states i.

The idea of the CPM [30,32] is to avoid the need to perform a self-consistent procedure for solution of Eqs. (1) and (2) by directly constructing the charge density $\rho(\mathbf{r})$. This is accomplished by assuming that the charge density in the neighborhood of a certain atom depends mainly on its local bonding environment. One then first performs full self-consistent DFT calculation on some small prototype system (see step 1 in Fig. 1) where atoms have the same bonding environment as in the large system. The charge density $\rho_s(\mathbf{r})$ obtained from such a calculation is then decomposed into contributions of individual atoms, called motifs (step 2 in Fig. 1), using the following formula:

$$m_A(\mathbf{r}-\mathbf{R}_A) = \frac{w_A(\mathbf{r}-\mathbf{R}_A)}{\sum_B w_B(\mathbf{r}-\mathbf{R}_B)}\rho_s(\mathbf{r}) . \tag{3}$$

In Eq. (3) $\mathbf{R}_A$ denotes the position of atom A, the summation in the denominator goes over all atoms in the system (labeled by B in the summation), while $w_A(\mathbf{r}-\mathbf{R}_A)$ are functions localized in the neighborhood of atom A that are used to smoothly partition the charge density $\rho_s(\mathbf{r})$ into motifs $m_A(\mathbf{r}-\mathbf{R}_A)$. The electronic charge density of atom A multiplied by a mask function $f_m(r)$ was used for w_A, where a mask function is of the form $f_m(r) = (a+br^2)/a$ when $r \le r_0$, and $f_m(r) = e^{-e_p r}/a$ when $r > r_0$, with $r_0 = 3\,a_0$ (where a_0 is the Bohr radius), $e_p = 0.75\,a_0{}^{-1}$, $b = -e_p\exp(-e_p r_0)/(2r_0)$, and $a = \exp(-e_p r_0) - br_0^2$. The motifs and atoms are classified based on the ideas used to classify the atoms used in classical force fields. For example, in the case of alkane chain, we introduce two types of C atoms – the atoms at ends of the chain are labeled as C_3, while the atoms in interior are labeled as C_2. The motif is then specified by the type of its central atom and its neighboring atoms, while in the case of hydrogen atom the second nearest neighbors also need to be specified to define the orientation of the motif in three-dimensional space. Previous experience has shown that such an approach is successful for a wide range of semiconducting systems. As an example, the following motifs are used in the case of alkanes:

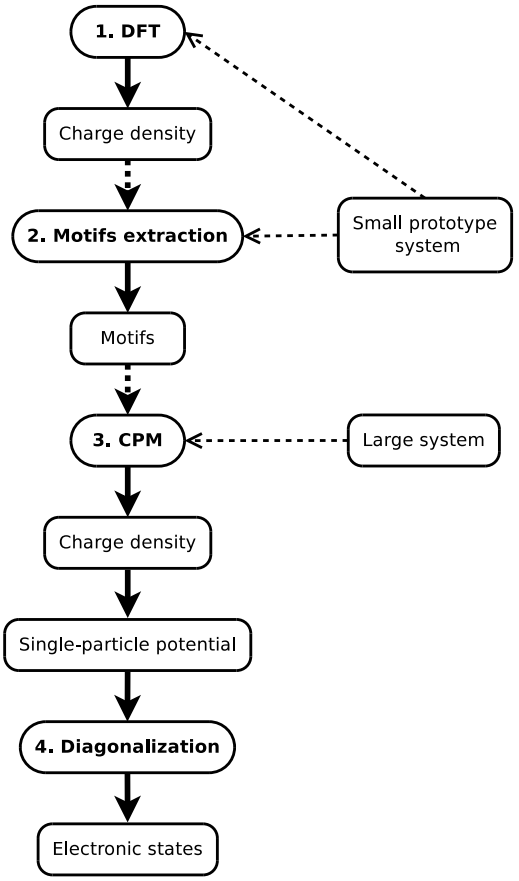

Fig. 1. CPM flow chart diagram shows the full CPM algorithm organized in phases. The first phase implements the DFT algorithm to calculate the charge density for the small prototype system. The charge density obtained from DFT is used in the second phase to extract the motifs. In the third phase, these motifs are used to calculate the electronic structure of the large system.

C_3–C_2HHH, C_2–C_3C_2HH, C_2–C_2C_2HH, H–C_3–C_2HH, H–C_2–C_3C_2H, and H–C_2–C_2C_2H. Other examples of the sets of motifs used for various physical systems are given in Table 1 of Supplementary material.

To obtain the charge density of the large system, one simply adds up the motifs of all atoms (step 3 in Fig. 1) as

$$\rho(\mathbf{r}) = \sum_A m_A \left[\mathcal{R}_A^{-1} \cdot (\mathbf{r} - \mathbf{R}_A)\right], \tag{4}$$

where $\mathcal{R}_A$ is the rotation matrix that takes into account that spatial orientation of neighboring atoms might not be the same in the small system used to generate the motifs and in the large system that one wants to calculate. In particular, if $\mathbf{R}_{A_i}$ are the positions of neighbors of atom A, while $\mathbf{R}_A^{(0)}$ and $\mathbf{R}_{A_i}^{(0)}$ are the positions of atom A and its neighbors in the motifs, then $\mathcal{R}_A \cdot \left(\mathbf{R}_{A_i}^{(0)} - \mathbf{R}_A^{(0)}\right) = \mathbf{R}_{A_i} - \mathbf{R}_A$. With electronic charge density at hand, one directly obtains the single-particle Hamiltonian [the term in bracket on the left hand side of Eq. (1)], which is then diagonalized (step 4 in Fig. 1) to obtain the energies and wave functions of electronic states.

In the case of plane wave implementation, diagonalization of this Hamiltonian can be computationally quite demanding for large systems because of large size of plane wave basis set and large number of eigenstates. Nevertheless, transport and optical properties of materials are determined only by electronic states in the vicinity of the band gap. It is therefore not necessary to find all eigenvalues in Eq. (1) but only those in the spectral region close to the band gap. Efficient methods for finding these eigenvalues, such as the folded spectrum method [34] and the overlapping fragments method [35] have been developed. The use of these methods on high performance computing architectures enabled the calculations of systems with more than 10 thousand atoms [36].

Comparisons of the results obtained by CPM and full DFT calculations for a variety of semiconducting systems have shown excellent agreement of the eigenvalues, which is on the order of 10–30 meV [32]. So far, CPM was applied to a variety of inorganic and organic semiconductor systems, such as diluted nitrogen alloys [30,37], quantum dots and wires [38,39], impurities [40,41], carbon nanotubes and fullerenes [31], amorphous polymers [42,36,43–45], thermally disordered polymers [46], as well as interfaces between domains in conjugated polymers [47] and small molecule based organic semi-

conductors [48]. On the other hand, CPM is not expected to work well in metals or systems where long-range charge transfer is present because the main assumption of locality of electronic charge density is not satisfied in these cases.

3. Implementation in Gaussian basis

To solve the eigenvalue problem given by Eq. (1), we expand the wave function $\psi_i(\mathbf{r})$ as a linear combination of predefined basis functions $\varphi_{k\mu}(\mathbf{r}-\mathbf{R}_k)$

$$\psi_i(\mathbf{r}) = \sum_{k=1}^{N}\sum_{\mu=1}^{N_k} \alpha_{k\mu}^{(i)} \varphi_{k\mu}(\mathbf{r}-\mathbf{R}_k). \tag{5}$$

In Eq. (1) N is the number of atoms in the system, N_k is the number of basis functions centered on atom k, $\mathbf{R}_k$ is the position of atom k, while $\alpha_{k\mu}^{(i)}$ are the expansion coefficients that have to be determined. Each of the basis functions is assumed in the form of a contracted Gaussian, i.e. as a linear combination of several primitive Gaussians

$$\varphi_{lmn}(\mathbf{r}) = \sum_j a_j \chi_{lmn\alpha_j}(\mathbf{r}) \tag{6}$$

with predefined coefficients a_j, where primitive Gaussians read

$$\chi_{lmn\alpha}(\mathbf{r}) = N(l,m,n,\alpha)\, x^l y^m z^n e^{-\alpha r^2}. \tag{7}$$

In Eq. (7) l, m and n are nonnegative integers and α is a positive real number, while $N(l,m,n,\alpha)$ is the normalization constant

$$N(l,m,n,\alpha) = \left(\frac{2\alpha}{\pi}\right)^{3/4} \sqrt{\frac{(8\alpha)^{l+m+n}\, l!\, m!\, n!}{(2l)!\,(2m)!\,(2n)!}}. \tag{8}$$

In the numerical examples in Sec. 4 we use the SBKJC VDZ ECP basis set [49–52].

Electronic charge density is also represented in the basis of contracted Gaussians centered on atoms as

$$\rho(\mathbf{r}) = \sum_{k=1}^{N}\sum_{\mu=1}^{n_k} \beta_{k\mu} \varphi_{k\mu}^{C}(\mathbf{r}-\mathbf{R}_k). \tag{9}$$

However, the set of Gaussians $\varphi_{k\mu}^{C}(\mathbf{r}-\mathbf{R}_k)$ used in Eq. (9) is different from the one used in Eq. (5) (a fact emphasized by the superscript C). The reasons for using different set of Gaussians stem from the fact that electronic charge density is equal to the sum of squared moduli of wave functions of occupied states. As a consequence, different parameters of Gaussians are needed to reliably represent the charge density than the ones used to represent the wave function. Hence, the number of Gaussians centered on atom k, denoted as n_k in Eq. (9), is different from N_k used in Eq. (5). In the numerical examples in Sec. 4 we use the DGauss A1 DFT Coulomb Fitting basis set [53,51,52]. Typically, n_k is larger than N_k. For example, in the case of carbon atom and the basis sets that we use in numerical examples in this work $n_k = 34$, while $N_k = 8$.

Appropriate representation of charge density motifs appears to be a significant challenge. Since the electronic charge density is represented as a sum of Gaussians centered on atoms, it is in some sense already decomposed into contributions of individual atoms. Therefore, it seems appealing to extract the motif from the calculation on small system simply as the sum of contributions of all Gaussians centered on that atom. In that case, the motif would be simply represented via the corresponding coefficients and it would be easy to generate the charge density of the large system from such motifs. Unfortunately, we found that this approach does not yield satisfactory results as the eigenenergies obtained using CPM differ too much to those obtained from full DFT calculation. The main reason for this stems from the fact that parameters of the Gaussian basis for charge density have been developed to provide a reliable fit of the total electronic charge density. Angular part of these Gaussians typically has only small angular momentum (typically s, p and d). On the other hand, the motifs that describe the neighborhood of a given atom exhibit a significant degree of anisotropy and consequently higher angular momentum Gaussians are needed to describe them.

Our next attempt in the effort to find an appropriate procedure to generate and represent the motifs was to use Eq. (3) to directly calculate the motif in a certain number of predefined points in real space and then to represent the obtained function as a linear combination of Gaussians. The set of Gaussians that was used is the same as the one used to represent the electronic charge density. The Gaussians used in the fit were centered on the central atom of the motif and on its neighbors. While the results obtained using this approach were better than in the previous case, they were still not satisfactory. We do not rule out the possibility that this approach could give better results with the use of different Gaussians, however that would require the development of appropriate Gaussian basis set, which would be a significant additional effort for a potential user of the CPM method.

Consequently, we decided to use a real space representation of the motifs. We calculate the values of the charge density motif using Eq. (3) and then store its values at points of a uniform real space grid of size $(2m_g+1)\times(2m_g+1)\times(2m_g+1)$ inside the cubic box of size $a\times a\times a$. In the numerical examples in Sec. 4 we use $m_g=80$ and $a=15\,a_0$. The center of the cubic box is at atomic position. In such an approach evaluation of charge density motifs using Eq. (3) is straightforward. However, it is a challenge to implement Eq. (4), i.e. to obtain the Gaussian basis representation of the electronic charge density from real space representation of motifs. We will describe in Sec. 3.3 how we address this challenge.

To obtain the eigenvalues and wave functions, we have to solve the generalized eigenvalue problem

$$\sum_{l\nu}\left(H_{k\mu,l\nu}-\varepsilon_i S_{k\mu,l\nu}\right)\alpha_{l\nu}^{(i)}=0 \tag{10}$$

where $S_{k\mu,l\nu}$ are the overlap matrix elements

$$S_{k\mu,l\nu}=\int \mathrm{d}^3\mathbf{r}\,\varphi_{k\mu}\left(\mathbf{r}-\mathbf{R}_k\right)\,\varphi_{l\nu}\left(\mathbf{r}-\mathbf{R}_l\right) \tag{11}$$

and $H_{k\mu,l\nu}$ are the single-particle Hamiltonian matrix elements. To evaluate the elements of this matrix, we need to calculate the kinetic integral

$$H^{(1)}_{k\mu,l\nu}=\int \mathrm{d}^3\mathbf{r}\,\varphi_{k\mu}\left(\mathbf{r}-\mathbf{R}_k\right)\left(-\frac{\hbar^2}{2m_0}\nabla^2\right)\varphi_{l\nu}\left(\mathbf{r}-\mathbf{R}_l\right), \tag{12}$$

the integral arising from the potential of nuclei and core electrons

$$H^{(2)}_{k\mu,l\nu}=\int \mathrm{d}^3\mathbf{r}\,\varphi_{k\mu}\left(\mathbf{r}-\mathbf{R}_k\right)\,V_{ion}\,\varphi_{l\nu}\left(\mathbf{r}-\mathbf{R}_l\right), \tag{13}$$

the Hartree integral

$$H^{(3)}_{k\mu,l\nu}=\int \mathrm{d}^3\mathbf{r}\,\varphi_{k\mu}\left(\mathbf{r}-\mathbf{R}_k\right)\,V_H\left[\rho\right]\,\varphi_{l\nu}\left(\mathbf{r}-\mathbf{R}_l\right), \tag{14}$$

and the exchange-correlation integral

$$H^{(4)}_{k\mu,l\nu}=\int \mathrm{d}^3\mathbf{r}\,\varphi_{k\mu}\left(\mathbf{r}-\mathbf{R}_k\right)\,V_{xc}\left[\rho\right]\,\varphi_{l\nu}\left(\mathbf{r}-\mathbf{R}_l\right). \tag{15}$$

In the following, we present our implementation of evaluation of each of these integrals.

3.1. Overlap and kinetic integral

A great convenience of Gaussian functions is that many relevant integrals that occur in electronic structure calculations can be calculated analytically. To calculate the kinetic [Eq. (12)] and overlap [Eq. (11)] integral, we have directly used the analytical formulas. Their form is given in our previous publication [54]. We refer the reader interested in their derivation to Ref. [55].

3.2. Nuclei and core electron integral

In this work, we employ the pseudopotential (also termed effective core potential) approach in which a certain number of core electrons is not treated explicitly but their effect is modeled using a pseudopotential operator. The contribution to operator V_{ion} in Eq. (13) from atom k is given as

$$V^k_{ion}=V^k_{pp}-\frac{Z_k e^2}{4\pi\,\varepsilon_0\cdot\left|\mathbf{r}-\mathbf{R}_k\right|}, \tag{16}$$

where $Z_k|e|$ includes the charge of nucleus and core electrons whose effect is modeled using a pseudopotential, while V^k_{pp} models all other effects of core electrons beyond the standard electrostatic effect. Therefore, for evaluation of matrix elements given in Eq. (13), one has to evaluate the nuclear attraction integrals

$$N_{k\mu,l\nu}=\int \mathrm{d}^3\mathbf{r}\,\varphi_{k\mu}\left(\mathbf{r}-\mathbf{R}_k\right)\,\frac{1}{\left|\mathbf{r}-\mathbf{R}_m\right|}\,\varphi_{l\nu}\left(\mathbf{r}-\mathbf{R}_l\right) \tag{17}$$

and the pseudopotential integrals

$$P_{k\mu,l\nu}=\int \mathrm{d}^3\mathbf{r}\,\varphi_{k\mu}\left(\mathbf{r}-\mathbf{R}_k\right)\,V^m_{pp}\,\varphi_{l\nu}\left(\mathbf{r}-\mathbf{R}_l\right). \tag{18}$$

We evaluate nuclear attraction integrals directly using analytical formulas [54,55]. To evaluate the integral with pseudopotentials, we follow the approach of Ref. [56]. In the numerical examples in Sec. 4 we use the pseudopotentials given in the SBKJC VDZ ECP basis set [49–52].

3.3. Hartree potential integral

Before one can evaluate the integrals that involve the electronic charge density $\rho(\mathbf{r})$, it is necessary first to represent $\rho(\mathbf{r})$ in the basis of Gaussian functions. To accomplish this, we choose a set of points in real space $\{\mathbf{r}_\alpha\}$ and corresponding weights w_α and evaluate $\rho(\mathbf{r}_\alpha)$ for each α using Eq. (4). To obtain the coefficients $\beta_{k\mu}$ in the Gaussian basis representation

$$\rho_f(\mathbf{r}) = \sum_{k\mu} \beta_{k\mu} \varphi^C_{k\mu}(\mathbf{r} - \mathbf{R}_k) \tag{19}$$

we minimize the expression

$$D = \sum_\alpha w_\alpha \left[\rho(\mathbf{r}_\alpha) - \rho_f(\mathbf{r}_\alpha)\right]^2, \tag{20}$$

with a constraint that the integral of charge density yields exactly the total valence electronic charge Q:

$$\int \mathrm{d}^3\mathbf{r}\, \rho_f(\mathbf{r}) = Q. \tag{21}$$

To perform the minimization with a previous constraint we use the method of Lagrange multipliers and minimize the functional

$$\mathcal{F}\left(\{\beta_{k\mu}\}, \lambda\right) = \sum_\alpha w_\alpha \left[\rho(\mathbf{r}_\alpha) - \rho_f(\mathbf{r}_\alpha)\right]^2 - \lambda \left[\sum_{k\mu} \beta_{k\mu} \int \mathrm{d}^3\mathbf{r}\, \varphi^C_{k\mu}(\mathbf{r} - \mathbf{R}_k) - Q\right]. \tag{22}$$

From the conditions $\frac{\partial \mathcal{F}}{\partial \beta_{k\mu}} = 0$ and $\frac{\partial \mathcal{F}}{\partial \lambda} = 0$ we obtain the following system of equations with unknowns $\beta_{k\mu}$ and λ:

$$\sum_{k\mu} q_{k\mu} \beta_{k\mu} = Q, \tag{23}$$

$$\sum_{l\nu} A_{k\mu,l\nu} \beta_{l\nu} - q_{k\mu} \lambda = B_{k\mu}, \tag{24}$$

where

$$q_{k\mu} = \int \mathrm{d}^3\mathbf{r} \varphi^C_{k\mu}(\mathbf{r} - \mathbf{R}_k), \tag{25}$$

$$A_{k\mu,l\nu} = 2 \sum_\alpha w_\alpha \varphi^C_{k\mu}(\mathbf{r}_\alpha - \mathbf{R}_k) \varphi^C_{l\nu}(\mathbf{r}_\alpha - \mathbf{R}_l), \tag{26}$$

and

$$B_{k\mu} = 2 \sum_\alpha w_\alpha \rho(\mathbf{r}_\alpha) \varphi^C_{k\mu}(\mathbf{r}_\alpha - \mathbf{R}_k). \tag{27}$$

The solution of the system of equations (23)–(24) yields the coefficients $\beta_{k\mu}$ [Eq. (19)], i.e. the Gaussian basis representation of the charge density. We use the same set of points in real space $\{\mathbf{r}_\alpha\}$ and corresponding weights w_α as the ones used for exchange-correlation integral calculation (see Sec. 3.4).

Next, we discuss our implementation of Hartree integral evaluation. Once the electronic charge density is represented in Gaussian basis, it is necessary to calculate the integrals

$$(ab|\, c) = \int \mathrm{d}^3\mathbf{r_1}\, \mathrm{d}^3\mathbf{r_2}\, \varphi_a(\mathbf{r_1}) \varphi_b(\mathbf{r_1}) \frac{1}{|\mathbf{r}_1 - \mathbf{r}_2|} \varphi^C_c(\mathbf{r_2}) \tag{28}$$

to obtain all matrix elements in Eq. (14). For brevity, we have introduced the notation $\varphi_a(\mathbf{r}) \equiv \varphi_{k_a\mu_a}\left(\mathbf{r} - \mathbf{R}_{k_a}\right)$ and similarly for $\varphi_b(\mathbf{r})$ and $\varphi^C_c(\mathbf{r})$.

The integral given in Eq. (28) is a special case of four-center Coulomb integral that occurs often in electronic structure calculations when one of the Gaussians is equal to a constant. This integral has an analytical solution whose form is given for example in [54,55]. One way to calculate all integrals given in Eq. (28) is simply to implement the analytical formula and use it to calculate each of the integrals. We have performed such an implementation and included it into our code.

However, due to somewhat lengthy form of the analytical expression, there are better alternatives which are based on the use of recurrence relations between the integrals [57]. In the four-integral case, an efficient scheme for calculation of all integrals was described in Ref. [58]. In what follows, we present a scheme for the three-integral case based on the ideas used in Ref. [58]. To this end we also introduce the notation for the integral over primitive Gaussians:

$$[ab|\ c] = \int \mathrm{d}^3\mathbf{r_1}\, \mathrm{d}^3\mathbf{r_2}\, \phi_a(\mathbf{r_1})\, \phi_b(\mathbf{r_1})\, \frac{1}{|\mathbf{r}_1 - \mathbf{r}_2|} \phi_c(\mathbf{r_2}) \tag{29}$$

where we use a brief notation for unnormalized primitive Gaussian centered at $\mathbf{A}$

$$\phi_a(\mathbf{r}) = (x - A_x)^{a_x} \left(y - A_y\right)^{a_y} (z - A_z)^{a_z}\, e^{-\alpha(\mathbf{r}-\mathbf{A})^2} \tag{30}$$

and similarly for ϕ_b and ϕ_c. The evaluation of integrals is based on the exploitation of recurrence relations

$$\begin{aligned}
[(a + 1_i)\, b|\ c]^{(m)} = {} & (P_i - A_i)\, [ab|\ c]^{(m)} + (W_i - P_i)\, [ab|\ c]^{(m+1)} + \\
& \frac{a_i}{2\xi} \left([(a - 1_i)\, b|\ c]^{(m)} - \frac{\gamma}{\xi + \gamma} [(a - 1_i)\, b|\ c]^{(m+1)} \right) + \\
& \frac{b_i}{2\xi} \left([a\,(b - 1_i)|\ c]^{(m)} - \frac{\gamma}{\xi + \gamma} [a\,(b - 1_i)|\ c]^{(m+1)} \right) + \\
& \frac{c_i}{2\,(\xi + \gamma)} [ab|\ c - 1_i]^{(m+1)}
\end{aligned} \tag{31}$$

and

$$(a\,(b + 1_i)|\ c) = ((a + 1_i)\, b|\ c) + (A_i - B_i)\, (ab|\ c)\,. \tag{32}$$

The symbols in Eqs. (31)–(32) have the following meaning. $[ab|\ c]^{(m)}$ is the auxiliary integral defined as

$$[ab|\ c]^{(m)} = \frac{2}{\sqrt{\pi}} \int_0^\infty \mathrm{d}u \left(\frac{u^2}{\rho + u^2} \right)^m \int \mathrm{d}^3\mathbf{r}_1\, \mathrm{d}^3\mathbf{r}_2\, \phi_a(\mathbf{r}_1)\, \phi_b(\mathbf{r}_1)\, e^{-u^2(\mathbf{r}_1 - \mathbf{r}_2)^2} \phi_c(\mathbf{r}_2)\,, \tag{33}$$

$\rho = \frac{(\alpha+\beta)\gamma}{\alpha+\beta+\gamma}$, $\xi = \alpha + \beta$, $\mathbf{P} = \frac{\alpha\mathbf{A}+\beta\mathbf{B}}{\alpha+\beta}$, $\mathbf{W} = \frac{\xi\mathbf{P}+\gamma\mathbf{C}}{\xi+\gamma}$ and the notation $(a \pm 1_i)$ denotes the Gaussian where the exponent a_i is increased/decreased by 1. One should also note that $[ab|\ c]^{(0)} = [ab|\ c]$.

From recurrence relation (32) it is evident that one can reduce the evaluation of $(ab|\ c)$ by repeated application of that relation to evaluation of integrals of the form $(a0_b|\ c)$ (the symbol 0_b denotes that $b_x = b_y = b_z = 0$). To evaluate $(a0_b|\ c)$ one needs to evaluate $[a0_b|\ c]^{(0)}$, which can further, by repeated application of Eq. (31), be reduced to evaluation of the integrals of the form $[0_a0_b|\ 0_c]^{(m)}$. The last integral is [58]

$$[0_a0_b|\ 0_c]^{(m)} = \frac{1}{\sqrt{\xi + \gamma}} K_{AB} K_C F_m(T)\,, \tag{34}$$

where $T = \frac{\xi\gamma}{\xi+\gamma} (\mathbf{P} - \mathbf{C})^2$, $F_m(T) = \int_0^1 t^{2m} e^{-Tt^2}\, \mathrm{d}t$, $K_{AB} = \frac{\sqrt{2}\pi^{5/4}}{\alpha+\beta} e^{-\frac{\alpha\beta}{\alpha+\beta}(\mathbf{A}-\mathbf{B})^2}$, $K_C = \frac{\sqrt{2}\pi^{5/4}}{\gamma}$.

There is a wealth of other ideas in the literature that have been used to efficiently calculate the integrals given in Eq. (28). One method is based on the generalization of the fast multipole method for the calculation of electrostatic energy between point charges to continuous charge distribution [59–61]. While this method yields formally linear scaling with system size, its applications are limited due to high prefactor and substantial amount of bookkeeping necessary for its implementation [60]. Other possibilities that are further from our approach (fully based on the use of Gaussians) are to represent the charge density in the basis of plane waves and exploit numerically efficient Fourier transform routines to calculate the integrals [62] or to make use of wavelet functions [63]. These possibilities will be further investigated in our future development of the parallel code.

3.4. Exchange-correlation integral

Due to nonlinear dependence of exchange-correlation potential V_{xc} on electronic charge density ρ, it is not possible to obtain analytical formulas for the exchange-correlation integral given in Eq. (15). We therefore perform numerical integration in real-space following Ref. [64], based on the ideas introduced in Ref. [65]. In brief, the space is smoothly partitioned into contributions from centers located on each atom. The partitioning function of Ref. [65] is used. To calculate the contribution of each center, numerical integration in spherical coordinates is performed. Lebedev grids [66] were used for integration over angular coordinates, while Chebyshev–Gauss grid transformed to the $0 < r < \infty$ interval [64] was used for radial integration. In the numerical examples in Sec. 4 we use the Lebedev grid with 74 points and the radial grid with 40 points and use the LDA exchange-correlation potential.

3.5. Truncation in the evaluation of integrals

Since Gaussian functions are well localized in space, integrals that contain products of Gaussians centered at different atoms that are spatially well separated are negligible. Consequently, their evaluation can be avoided. We exploit this fact to reduce the computational effort.

In particular, to define a systematic criterion whether a certain integral should be evaluated or not, we define the radius of the contracted Gaussian as the largest r_g that satisfies the criterion

$$\sum_j a_j N\left(l,m,n,\alpha_j\right) r_g^{l+m+n} e^{-\alpha_j {r_g}^2} = \varepsilon. \tag{35}$$

With such a choice of r_g it is guaranteed that $|\varphi_{lmn}(\mathbf{r})| < \varepsilon$ when $r > r_g$, i.e. that the Gaussian will have a value smaller than ε outside the sphere of radius r_g. Next, for each two Gaussians we check if the distance between their centers is larger than the sum of their radii. If this is the case, then we exclude from calculation all integrals that involve the product of these two Gaussians.

Such a truncation procedure reduces the number of overlap [Eq. (11)], kinetic [Eq. (12)] and exchange-correlation [Eq. (15)] integrals that have to be calculated from $O\left(N^2\right)$ to $O(N)$. The number of nuclear attraction integrals [Eq. (17)], the pseudopotential integrals [Eq. (18)] and the Hartree integrals [Eq. (28)] is reduced from $O\left(N^3\right)$ to $O\left(N^2\right)$. Consequently, by exploitation of Gaussian function locality, the overall computational effort is reduced from $O\left(N^3\right)$ to $O\left(N^2\right)$. It is possible to further reduce the computational effort by exploiting the decay of Coulomb $\frac{1}{|\mathbf{r}-\mathbf{R}_a|}$ term, which was not yet exploited in our implementation.

In the numerical examples in Sec. 4 we use $\varepsilon = 10^{-4}\, {a_0}^{-3/2}$. Such a truncation introduces eigenenergy errors less than 0.1 mHa.

3.6. Diagonalization of the Hamiltonian

After all integrals are evaluated, one has to solve the generalized eigenvalue problem given in Eq. (10). In the current single-processor implementation we simply perform the diagonalization using the standard single-processor LAPACK routines [67].

A big advantage of Gaussian basis is that one can accurately represent the wave function with a relatively small number of Gaussians per atom. For example, the SBKJC VDZ ECP basis set that we use in the numerical example in Sec. 4 contains 8 Gaussians per Si atom and 2 Gaussians per H atom. Consequently, even for the largest $Si_{837}H_{348}$ system that we used for testing the code, the dimension of the corresponding Hamiltonian matrix is 7392×7392. Therefore, its diagonalization using LAPACK takes only a small portion of total computational time.

In future development of the parallel code that will be aimed at tackling even larger systems, direct diagonalization might become a limiting step due to its N^3 scaling with system size. In this case, the sparsity of the matrix can be exploited, or the diagonalization methods such as the folded spectrum method [34] and the overlapping fragments method [35], to obtain reduced computational time and more favorable scaling with system size.

4. Performance and validation of implemented code

The algorithm described in Sec. 3 was implemented in C programming language. Its performance was then tested on a computer with Core i7 5820k CPU and 64 GB DDR4 RAM. C code was compiled with the GNU C Compiler (GCC) and executed on the Linux operation system. The tests were performed on different physical systems such as alkane oligomers (Fig. 2a), thiophene oligomers [without substitution (Fig. 2b) and with substitution of hydrogen atom by fluorine (Fig. 2e) or chlorine (Fig. 2d)], silicon nanocrystals (Fig. 2f), furane oligomers (Fig. 2c), disordered poly(3-hexylthiophene) (P3HT) chains (Fig. 2h) and array of polythiophene chains (Fig. 2i). The choice of systems was made to perform the test on one-, two- and three- dimensional systems, to consider both organic and inorganic systems, to include chemical elements from various groups of periodic table, as well as to include both ordered and disordered systems.

First, we compare the results obtained by DFT and CPM to confirm previous conclusions from plane-wave code that CPM yields the eigenvalues with accuracy comparable to the one of DFT. The comparisons were made for several different classes of insulating and semiconducting systems – alkane oligomers C_nH_{2n+2} with $n = 10$, $n = 20$ and $n = 40$, thiophene oligomers $C_{4n}S_nH_{2n+2}$ with $n = 3$, $n = 4$ and $n = 7$, array of thiophene oligomers $(C_{4n}S_nH_{2n+2})_m$ with $(n, m) = (3, 3)$; $(3, 4)$; $(4, 3)$; $(4, 4)$, silicon nanocrystals $Si_{29}H_{36}$, $Si_{35}H_{36}$ and $Si_{59}H_{60}$, furane oligomers $C_{4n}O_nH_{2n+2}$ with $n = 3$, $n = 4$, $n = 5$, $n = 6$ and $n = 8$, thiophene oligomers where one hydrogen atom is substituted with chlorine ($C_{4n}S_nCl_nH_{n+2}$ with $n = 3$, $n = 4$, and $n = 6$) or fluorine ($C_{4n}S_nF_nH_{n+2}$ with $n = 3$, $n = 4$, and $n = 6$), boron-nitride nanoflakes $B_{19}N_{19}H_{16}$, $B_{27}N_{27}H_{20}$ and $B_{34}N_{34}H_{22}$, and disordered P3HT with 77, 102 and 152 atoms. The list of atom types and motifs used for each system is presented in Table 1 in Supplementary material. For illustration, the results obtained for alkane oligomers (C_nH_{2n+2}) with $n = 10$, $n = 20$ and $n = 40$ are shown in Table 1, where the eigenenergies of ten highest occupied states are presented. The motifs were generated from DFT calculation of the $C_{10}H_{22}$ molecule and then used in CPM calculation for all system sizes. The results presented in Table 1 indicate that the difference between eigenenergies obtained by DFT and CPM

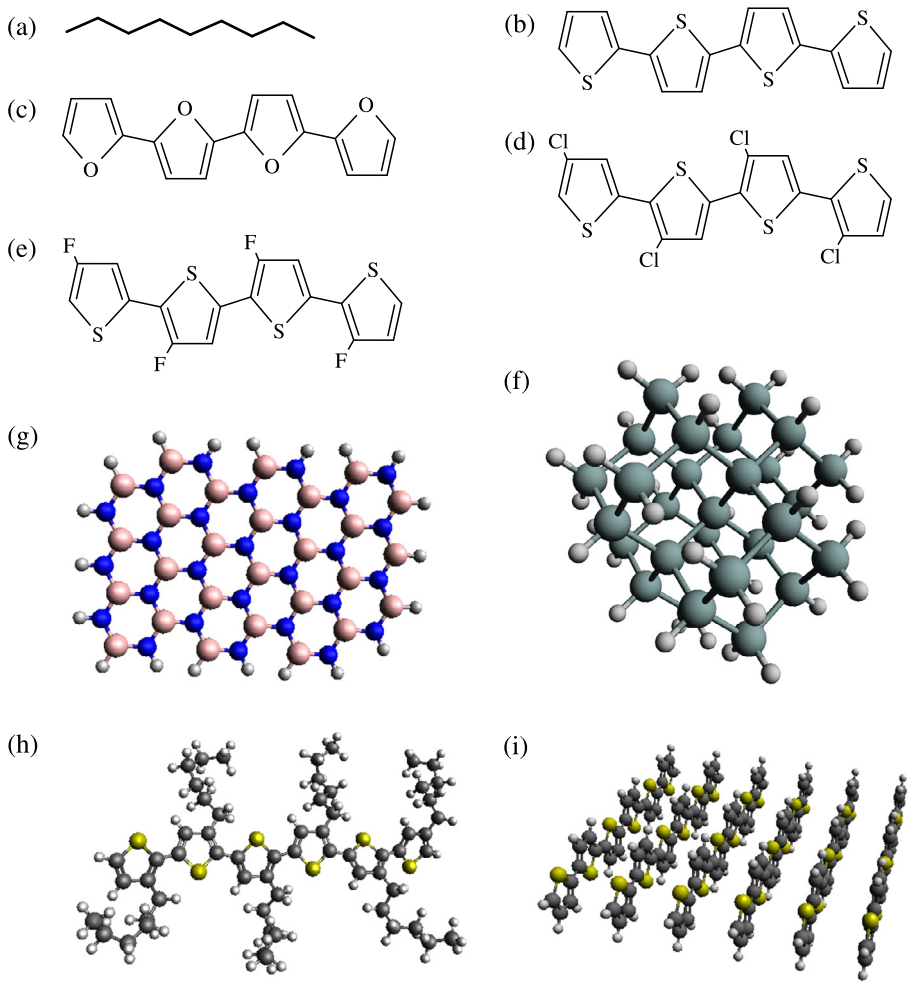

Fig. 2. Structural or atomic representation of physical systems used to test the code: (a) alkane oligomers; (b) thiophene oligomers; (c) furane oligomers; (d) chlorine substituted thiophene oligomers; (e) fluorine substituted thiophene oligomers; (f) silicon nanocrystals; (g) boron-nitride nanoflakes; (h) disordered poly(3-hexylthiophene); (i) array of polythiophene chains.

Table 1
Comparison of eigenenergies (in Ha) of $C_{10}H_{22}$, $C_{20}H_{42}$ and $C_{40}H_{82}$ obtained by Gaussian basis implementations of CPM and DFT.

$C_{10}H_{22}$		$C_{20}H_{42}$		$C_{40}H_{82}$	
CPM	DFT	CPM	DFT	CPM	DFT
−0.309603	−0.309024	−0.278819	−0.278651	−0.275738	−0.276441
−0.290277	−0.289713	−0.278804	−0.278263	−0.275696	−0.276399
−0.290144	−0.289644	−0.278742	−0.277949	−0.275376	−0.275761
−0.281836	−0.281425	−0.278170	−0.277590	−0.275333	−0.275743
−0.279675	−0.279398	−0.276962	−0.276825	−0.267867	−0.268255
−0.279312	−0.278751	−0.276230	−0.275420	−0.252784	−0.253185
−0.278589	−0.277850	−0.275932	−0.275314	−0.239152	−0.239529
−0.276855	−0.276513	−0.261474	−0.260857	−0.227590	−0.227898
−0.275733	−0.275079	−0.235925	−0.235267	−0.218769	−0.218922
−0.230841	−0.229995	−0.218384	−0.217236	−0.213411	−0.213216

is typically less than 1 mHa. To verify the accuracy of CPM for a wider class of systems, for each of the investigated systems we calculate the mean square difference of eigenenergies of occupied states obtained from CPM and DFT. The results obtained are presented in Table 2. The results suggest that eigenenergy error is on the order of 1 mHa. Consequently, CPM yields the eigenenergies which can be considered to be as accurate as the ones obtained from DFT.

Next, we discuss memory limitations of our CPM implementation. We store full matrices H and S in memory. Their largest dimension for the systems considered in this work is 7392×7392 in the case of $Si_{837}H_{348}$ nanocrystal and these

Table 2
Mean square difference $\delta\varepsilon = \sqrt{\langle(\Delta\varepsilon)^2\rangle}$ of occupied state eigenenergies obtained using Gaussian basis CPM and DFT for different systems investigated in this work.

System	$C_{10}H_{22}$	$C_{20}H_{42}$	$C_{40}H_{82}$	$C_{12}S_3H_8$	$C_{16}S_4H_{10}$	$C_{28}S_7H_{16}$
$\delta\varepsilon$ (mHa)	0.58	0.58	0.64	0.58	0.36	0.55
System	$Si_{29}H_{36}$	$Si_{35}H_{36}$	$Si_{59}H_{60}$	$C_{12}S_3Cl_3H_5$	$C_{16}S_4Cl_4H_6$	$C_{24}S_6Cl_6H_8$
$\delta\varepsilon$ (mHa)	1.8	0.50	2.1	1.0	1.4	1.8
System	$C_{12}O_3H_8$	$C_{16}O_4H_{10}$	$C_{20}O_5H_{12}$	$C_{24}O_6H_{14}$	$C_{32}O_8H_{18}$	$(C_{12}S_3H_8)_3$
$\delta\varepsilon$ (mHa)	1.4	1.6	2.0	1.8	2.0	0.69
System	$(C_{12}S_3H_8)_4$	$(C_{16}S_4H_{10})_3$	$(C_{16}S_4H_{10})_4$	$C_{12}S_3F_3H_5$	$C_{16}S_4F_4H_6$	$C_{24}S_6F_6H_8$
$\delta\varepsilon$ (mHa)	0.74	0.89	1.3	0.65	0.82	1.5
System	$B_{19}N_{19}H_{16}$	$B_{27}N_{27}H_{20}$	$B_{34}N_{34}H_{22}$	d-P3HT-77	d-P3HT-102	d-P3HT-152
$\delta\varepsilon$ (mHa)	1.1	1.1	1.3	3.5	3.6	3.4

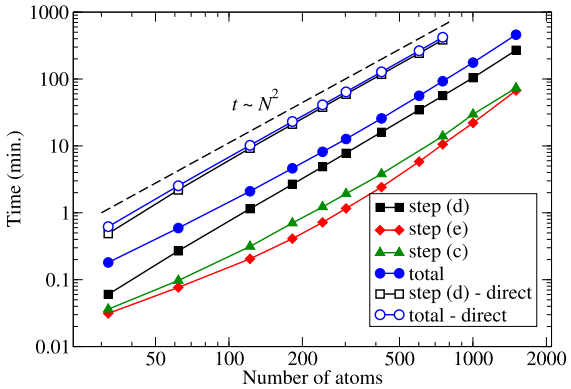

Fig. 3. Dependence of computational time for alkane oligomers on the number of atoms for most time-consuming parts of the code: step (c) – reading of motifs and calculation of Gaussian basis representation of charge density (full triangles); step (d) – calculation of Hartree potential integrals in two cases – using recurrence formulas (full squares) or direct analytical formulas (empty squares); step (e) – calculation of exchange-correlation integrals (diamonds); and total time in two different cases for step (d) (full circles and empty circles). The dashed line showing $t \sim N^2$ dependence is given as a guide to the eye.

matrices consume most of the memory. Nevertheless, these can safely be stored in the RAM of a single machine and we have not exploited the sparsity of these matrices in the present implementation. In future implementation for parallel machines, these matrices will have to be distributed over nodes or their sparsity could be exploited. We note that the number of three center Hartree integrals $(ab|\ c)$ [Eq. (28)] is rather large ($N_b^2 N_c$, where N_b is the total size of the wave function basis set and N_c is the total size of the basis set for charge density) and these can not be stored in RAM for larger systems. Fortunately, in CPM, once a certain Hartree integral is calculated, it can be added to the corresponding element of the H matrix and there is no need to store it in memory.

Next, we analyze the scaling of the computational time with system size and the contribution of different parts of the code to the total time. For the latter, we consider the following main parts of the program: (a) calculation of kinetic, overlap and nuclear attraction integrals; (b) calculation of pseudopotential integrals; (c) reading of motifs and calculation of Gaussian basis representation of charge density; (d) calculation of Hartree potential integrals; (e) calculation of exchange-correlation integrals; (f) diagonalization of the Hamiltonian. Part (d) was implemented using two different approaches – the direct approach based on analytical formulas and the approach based on recurrence formulas that was described in Sec. 3.3. Consequently, we present the computational times in both cases. We find that three parts of the code that are most time consuming are parts (c), (d), (e) and we present their computational times for alkane oligomers in Fig. 3. Total time, as well as times for each of the parts (c), (d) and (e) scale as $t \sim N^2$ for larger values of N. In the case of Hartree potential integrals [step (d)], this scaling comes from the fact that the number of integrals that has to be calculated scales as $O(N^2)$. In parts (c) and (e) it comes from the fact that one needs to calculate electronic charge density and Gaussians in each point of real space grid. Fig. 3 shows that the computational time is dominated by step (d). For this reason, we have made a significant effort to optimize the execution of this step as much as possible, as described in Sec. 3.3. In Fig. 3 we also present the time for step (d) and the total time when Hartree integrals are evaluated directly using analytical formulas. These results suggest that a significant decrease of computational time was obtained by employing the recurrence formulas.

In Fig. 4 we present the scaling of computational time with system size for systems of different dimensionality: one-dimensional alkane oligomers, two-dimensional array of thiophene oligomers and three-dimensional silicon nanocrystals. The results demonstrate that it is more demanding to perform the calculations for systems of higher dimensionality. Such a dependence originates from the fact that in higher dimensional systems each atom has more neighbors and therefore

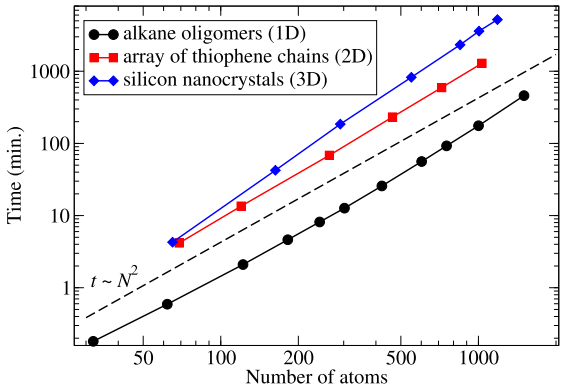

Fig. 4. Dependence of computational time of the CPM code on the number of atoms for alkane oligomers, two-dimensional array of polythiophene chains and three-dimensional silicon nanocrystals. The dashed line showing $t \sim N^2$ dependence is given as a guide to the eye.

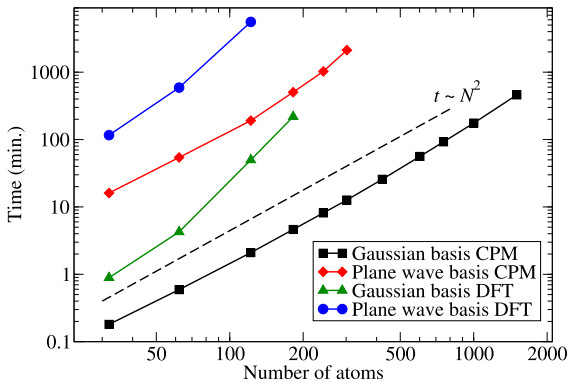

Fig. 5. Comparison of the dependence of computational time on the number of atoms of alkane oligomers for Gaussian basis and plane wave basis DFT and CPM codes. The dashed line showing $t \sim N^2$ dependence is given as a guide to the eye.

the number of integrals that need to be calculated and include basis functions of that atom is larger. Nevertheless, the systems with as much as thousand atoms can be calculated in the time on the order of hours on a single processor machine. We note that the computational time scales as $\sim N^2$ in the case of one- and two-dimensional systems. In the case of three-dimensional silicon nanocrystals the scaling is somewhat worse in the range of sizes investigated here. Such a scaling originates from the fact that for these small sizes the number of integrals that has to be calculated does not yet reach the large N limit of $\sim N^2$.

In Fig. 5 we compare the computational time of the developed Gaussian basis CPM code with previous plane wave based implementation for the case of alkane oligomers. In the plane wave based code the most time consuming part is the diagonalization of the Hamiltonian, while the construction of the electronic charge density and the single-particle potential take only a minor part of the computational time. The times reported in Fig. 5 were obtained by performing the diagonalization using the conjugate gradient algorithm, as implemented in the ESCAN [34] code. On the other hand, in Gaussian basis code the most time-consuming part is the construction of the Hamiltonian (in particular the Hartree potential contribution, as already discussed), while its diagonalization takes only a negligible part of computational time due to small size of the Gaussian basis set. Small size of the Gaussian basis set is the main origin of superior performance of Gaussian basis code that enables calculation of alkane systems with as much as 1500 atoms using a single CPU core in just several hours, as can be seen in Fig. 5. We also note that our results for computational times are in-line with previously known facts that the construction of the Hamiltonian, i.e. the calculation of Gaussian integrals is the rate-limiting step in electronic structure calculations in Gaussian basis [58,61,59,62], while diagonalization of the Hamiltonian using conjugate gradient techniques is the rate-limiting step in plane-wave based calculations [3]. Furthermore, since we have established in this work that Gaussian basis CPM results agree well with Gaussian basis DFT results and it has been previously established [32] that plane wave based DFT and CPM results agree well, it is expected that the difference between Gaussian basis CPM and plane wave basis CPM will originate mainly from different basis sets and that it will be relatively small. This is confirmed by the results for the eigenenergy difference obtained by these two approaches that is presented in Table 2 of Supplementary material. This is typical difference obtained due to difference between Gaussian and plane wave basis sets and due to slight difference in pseudopotentials used in the two cases.

In Fig. 5 we also present the comparison of DFT and CPM computational time both for Gaussian basis and plane wave codes in the case of alkane oligomers. The PETOT [7] plane wave DFT code and our implementation of Gaussian basis DFT were used in the computation. The main advantage of CPM over full DFT calculation is that one avoids the iterations needed to reach a self-consistent solution of Eqs. (1) and (2). Therefore, one can roughly expect that the time for the DFT code will be number of iterations times larger than the time for CPM code. This is not entirely the case for Gaussian basis code where one can avoid the repetition of some calculations that are common for each DFT iteration. For example, calculation of Hartree integrals which is the most time consuming step does not have to be repeated in every DFT iteration because the same integrals are calculated. On the other hand, calculation of exchange-correlation integrals has to be repeated because the electronic charge density is different in different iterations. In addition, DFT code also contains implementation of Eq. (2) which takes a significant portion of time in Gaussian basis. As a consequence of all these considerations, we find that our Gaussian basis CPM code is at least five times faster than our DFT code, see Fig. 5, while the number of DFT iterations was between 20 and 35 for these systems. For larger systems (between 100 and 200 atoms) the ratio of computational times becomes even bigger, mainly due to time needed for evaluation of Eq. (2). Moreover, we note that it is not possible to store all Hartree integrals for very large systems due to memory limitations and in this case one needs to recalculate these in each DFT iteration. Therefore, for such systems Gaussian basis CPM would indeed become at least number of iteration times faster than Gaussian basis DFT. In Figs. 2 and 3 in Supplementary material we present the comparison of the performance of DFT and CPM Gaussian basis and plane wave codes for arrays of polythiophene chains and for silicon nanocrystals which can respectively be considered as representatives of two-dimensional and three-dimensional systems. We find that general conclusions regarding the comparison of the performance of the codes remain the same in these cases as well.

5. Conclusion

In conclusion, we presented the Gaussian basis implementation of the charge patching method for electronic structure calculations. We put focus on the steps that are not present in Gaussian basis implementations of DFT. In particular, we found that the most convenient way to store the charge density motifs is to use a uniform real space grid. Consequently, we developed the method to obtain the Gaussian basis representation of the electronic charge density from motifs represented in real space. We also present the recurrence scheme for evaluation of Hartree three-center integrals based on the modification of previous schemes with four-center integrals. With such a scheme, a significantly better performance of the code is obtained than in the case when integrals are calculated directly using analytical formulas. Performance tests of serial version of the code indicate that systems with several hundreds of atoms can be calculated in less than an hour and we achieved to calculate the system with as much as 1500 atoms on a single processor with computational time of several hours.

Further work on the code will be focused on development of its parallel version. The ability to treat systems with more than one thousand atoms using a serial version on a single CPU core implies that parallelization should enable calculations of systems with tens of thousands atoms on modest size computing clusters with several hundreds of CPU cores.

Acknowledgements

The authors would like to thank Marko Mladenović for providing input coordinates of disordered P3HT chains.

NV gratefully acknowledges the support by the Ministry of Education, Science and Technological Development of the Republic of Serbia (Project No. ON171017) and the European Commission under H2020 project VI-SEEM, Grant No. 675121, as well as the contribution of the COST Action MP1406. SS and BZ acknowledge support by the SCOPES project no. IZ74Z0-160453.

Appendix A. Supplementary material

Supplementary material related to this article can be found online at https://doi.org/10.1016/j.jcp.2018.04.032.

References

[1] P. Hohenberg, W. Kohn, Inhomogeneous electron gas, Phys. Rev. 136 (1964) B864.
[2] W. Kohn, L.J. Sham, Self-consistent equations including exchange and correlation effects, Phys. Rev. 140 (1965) A1133.
[3] M.C. Payne, M.P. Teter, D.C. Allan, T.A. Arias, J.D. Joannopoulos, Iterative minimization techniques for ab initio total-energy calculations: molecular dynamics and conjugate gradients, Rev. Mod. Phys. 64 (1992) 1045.
[4] P. Giannozzi, S. Baroni, N. Bonini, M. Calandra, R. Car, C. Cavazzoni, D. Ceresoli, G.L. Chiarotti, M. Cococcioni, I. Dabo, A. Dal Corso, S. de Gironcoli, S. Fabris, G. Fratesi, R. Gebauer, U. Gerstmann, C. Gougoussis, A. Kokalj, M. Lazzeri, L. Martin-Samos, N. Marzari, F. Mauri, R. Mazzarello, S. Paolini, A. Pasquarello, L. Paulatto, C. Sbraccia, S. Scandolo, G. Sclauzero, A.P. Seitsonen, A. Smogunov, P. Umari, R.M. Wentzcovitch, QUANTUM ESPRESSO: a modular and open-source software project for quantum simulations of materials, J. Phys. Condens. Matter 21 (2009) 395502.
[5] X. Gonze, B. Amadon, P.-M. Anglade, J.-M. Beuken, F. Bottin, P. Boulanger, F. Bruneval, D. Caliste, R. Caracas, M. Côté, T. Deutsch, L. Genovese, P. Ghosez, M. Giantomassi, S. Goedecker, D. Hamann, P. Hermet, F. Jollet, G. Jomard, S. Leroux, M. Mancini, S. Mazevet, M. Oliveira, G. Onida, Y. Pouillon, T. Rangel, G.-M. Rignanese, D. Sangalli, R. Shaltaf, M. Torrent, M. Verstraete, G. Zerah, J. Zwanziger, Abinit: first-principles approach to material and nanosystem properties, Comput. Phys. Commun. 180 (2009) 2582.
[6] S.J. Clark, M.D. Segall, C.J. Pickard, P.J. Hasnip, M.J. Probert, K. Refson, M.C. Payne, First principles methods using CASTEP, Z. Kristallogr. 220 (2005) 567.

[7] PETOT, http://cmsn.lbl.gov/html/PEtot/PEtot.html, last accessed 4 April 2018.
[8] M. Valiev, E. Bylaska, N. Govind, K. Kowalski, T. Straatsma, H.V. Dam, D. Wang, J. Nieplocha, E. Apra, T. Windus, W. de Jong, NWChem: a comprehensive and scalable open-source solution for large scale molecular simulations, Comput. Phys. Commun. 181 (2010) 1477.
[9] M.J. Frisch, G.W. Trucks, H.B. Schlegel, G.E. Scuseria, M.A. Robb, J.R. Cheeseman, G. Scalmani, V. Barone, B. Mennucci, G.A. Petersson, H. Nakatsuji, M. Caricato, X. Li, H.P. Hratchian, A.F. Izmaylov, J. Bloino, G. Zheng, J.L. Sonnenberg, M. Hada, M. Ehara, K. Toyota, R. Fukuda, J. Hasegawa, M. Ishida, T. Nakajima, Y. Honda, O. Kitao, H. Nakai, T. Vreven, J.A. Montgomery Jr., J.E. Peralta, F. Ogliaro, M. Bearpark, J.J. Heyd, E. Brothers, K.N. Kudin, V.N. Staroverov, R. Kobayashi, J. Normand, K. Raghavachari, A. Rendell, J.C. Burant, S.S. Iyengar, J. Tomasi, M. Cossi, N. Rega, J.M. Millam, M. Klene, J.E. Knox, J.B. Cross, V. Bakken, C. Adamo, J. Jaramillo, R. Gomperts, R.E. Stratmann, O. Yazyev, A.J. Austin, R. Cammi, C. Pomelli, J.W. Ochterski, R.L. Martin, K. Morokuma, V.G. Zakrzewski, G.A. Voth, P. Salvador, J.J. Dannenberg, S. Dapprich, A.D. Daniels, O. Farkas, J.B. Foresman, J.V. Ortiz, J. Cioslowski, D.J. Fox, in: Gaussian 09, Gaussian Inc., Wallingford CT, 2009.
[10] J.M. Soler, E. Artacho, J.D. Gale, A. García, J. Junquera, P. Ordejón, D. Sánchez-Portal, The SIESTA method for ab initio order N materials simulation, J. Phys. Condens. Matter 14 (2002) 2745.
[11] L. Kronik, A. Makmal, M.L. Tiago, M.M.G. Alemany, M. Jain, X. Huang, Y. Saad, J.R. Chelikowsky, PARSEC – the pseudopotential algorithm for real-space electronic structure calculations: recent advances and novel applications to nano-structures, Phys. Status Solidi B 243 (2006) 1063.
[12] V. Michaud-Rioux, L. Zhang, H. Guo RESCU, A real space electronic structure method, J. Comput. Phys. 307 (2016) 593.
[13] A.S. Banerjee, R.S. Elliott, R.D. James, A spectral scheme for Kohn–Sham density functional theory of clusters, J. Comput. Phys. 287 (2015) 226.
[14] J. Deslippe, G. Samsonidze, D.A. Strubbe, M. Jain, M.L. Cohen, S.G. Louie, BerkeleyGW: a massively parallel computer package for the calculation of the quasiparticle and optical properties of materials and nanostructures, Comput. Phys. Commun. 183 (2012) 1269.
[15] A.J. Garza, G.E. Scuseria, Predicting band gaps with hybrid density functionals, J. Phys. Chem. Lett. 7 (2016) 4165.
[16] M. Aldegunde, J.R. Kermode, N. Zabaras, Development of an exchange-correlation functional with uncertainty quantification capabilities for density functional theory, J. Comput. Phys. 311 (2016) 173.
[17] G. Kotliar, S.Y. Savrasov, K. Haule, V.S. Oudovenko, O. Parcollet, C.A. Marianetti, Electronic structure calculations with dynamical mean-field theory, Rev. Mod. Phys. 78 (2006) 865.
[18] W. Hu, L. Lin, C. Yang, DGDFT: a massively parallel method for large scale density functional theory calculations, J. Chem. Phys. 143 (2015) 124110.
[19] T.V.T. Duy, T. Ozaki, A three-dimensional domain decomposition method for large-scale DFT electronic structure calculations, Comput. Phys. Commun. 185 (2014) 777.
[20] S. Mohr, L.E. Ratcliff, L. Genovese, D. Caliste, P. Boulanger, S. Goedecker, T. Deutsch, Accurate and efficient linear scaling DFT calculations with universal applicability, Phys. Chem. Chem. Phys. 17 (2015) 31360.
[21] Y. Pan, X. Dai, S. de Gironcoli, X.-G. Gong, G.-M. Rignanese, A. Zhou, A parallel orbital-updating based plane-wave basis method for electronic structure calculations, J. Comput. Phys. 348 (2017) 482.
[22] E. Vecharynski, C. Yang, J.E. Pask, A projected preconditioned conjugate gradient algorithm for computing many extreme eigenpairs of a hermitian matrix, J. Comput. Phys. 290 (2015) 73.
[23] M. Lee, K. Leiter, C. Eisner, J. Knap, Atom-partitioned multipole expansions for electrostatic potential boundary conditions, J. Comput. Phys. 328 (2017) 344.
[24] G. Zhang, L. Lin, W. Hu, C. Yang, J.E. Pask, Adaptive local basis set for Kohn–Sham density functional theory in a discontinuous Galerkin framework II: force, vibration, and molecular dynamics calculations, J. Comput. Phys. 335 (2017) 426.
[25] D. Porezag, T. Frauenheim, T. Köhler, G. Seifert, R. Kaschner, Construction of tight-binding-like potentials on the basis of density-functional theory: application to carbon, Phys. Rev. B 51 (1995) 12947.
[26] M. Elstner, D. Porezag, G. Jungnickel, J. Elsner, M. Haugk, T. Frauenheim, S. Suhai, G. Seifert, Self-consistent-charge density-functional tight-binding method for simulations of complex materials properties, Phys. Rev. B 58 (1998) 7260.
[27] K. Kitaura, E. Ikeo, T. Asada, T. Nakano, M. Uebayasi, Fragment molecular orbital method: an approximate computational method for large molecules, Chem. Phys. Lett. 313 (1999) 701.
[28] L.-W. Wang, A. Zunger, Local-density-derived semiempirical pseudopotentials, Phys. Rev. B 51 (1995) 17398.
[29] H. Fu, A. Zunger, Local-density-derived semiempirical nonlocal pseudopotentials for InP with applications to large quantum dots, Phys. Rev. B 55 (1997) 1642.
[30] L.-W. Wang, Charge-density patching method for unconventional semiconductor binary systems, Phys. Rev. Lett. 88 (2002) 256402.
[31] L.-W. Wang, Generating charge densities of fullerenes, Phys. Rev. B 65 (2002) 153410.
[32] N. Vukmirović, L.-W. Wang, Charge patching method for electronic structure of organic systems, J. Chem. Phys. 128 (2008) 121102.
[33] C. Huang, Patching the exchange-correlation potential in density functional theory, J. Chem. Theory Comput. 12 (2016) 2224.
[34] A. Canning, L.W. Wang, A. Williamson, A. Zunger, Parallel empirical pseudopotential electronic structure calculations for million atom systems, J. Comput. Phys. 160 (2000) 29.
[35] N. Vukmirović, L.-W. Wang, Overlapping fragments method for electronic structure calculation of large systems, J. Chem. Phys. 134 (2011) 094119.
[36] N. Vukmirović, L.-W. Wang, Density of states and wave function localization in disordered conjugated polymers: a large scale computational study, J. Phys. Chem. B 115 (2011) 1792.
[37] L.-W. Wang, Large-scale local-density-approximation band gap-corrected GaAsN calculations, Appl. Phys. Lett. 78 (2001) 1565.
[38] J. Li, L.-W. Wang, Band-structure-corrected local density approximation study of semiconductor quantum dots and wires, Phys. Rev. B 72 (2005) 125325.
[39] D.J. Milliron, S.M. Hughes, Y. Cui, L. Manna, J. Li, L.W. Wang, A.P. Alivisatos, Colloidal nanocrystal heterostructures with linear and branched topology, Nature (London) 430 (2004) 190.
[40] J. Li, L.-W. Wang, Energy levels of isoelectronic impurities by large scale LDA calculations, Phys. Rev. B 67 (2003) 033102.
[41] J. Li, L.-W. Wang, First principles calculations of ZnS:Te energy levels, Phys. Rev. B 67 (2003) 205319.
[42] N. Vukmirović, L.-W. Wang, Electronic structure of disordered conjugated polymers: polythiophenes, J. Phys. Chem. B 113 (2009) 409.
[43] N. Vukmirović, L.-W. Wang, Charge carrier motion in disordered conjugated polymers: a multiscale ab initio study, Nano Lett. 9 (2009) 3996.
[44] N. Vukmirović, L.-W. Wang, Carrier hopping in disordered semiconducting polymers: How accurate is the Miller–Abrahams model? Appl. Phys. Lett. 97 (2010) 043305.
[45] J. Granadino-Roldan, N. Vukmirović, M. Fernandez-Gomez, L.-W. Wang, The role of disorder on the electronic structure of conjugated polymers. The case of poly-2, 5-bis(phenylethynyl)-1, 3,4-thiadiazole, Phys. Chem. Chem. Phys. 13 (2011) 14500.
[46] M. Mladenović, N. Vukmirović, Effects of thermal disorder on the electronic properties of ordered polymers, Phys. Chem. Chem. Phys. 16 (2014) 25950–25958.
[47] M. Mladenović, N. Vukmirović, Electronic states at the interface between crystalline and amorphous domains in conjugated polymers, J. Phys. Chem. C 119 (2015) 23329.
[48] M. Mladenović, N. Vukmirović, I. Stanković, Electronic states at low-angle grain boundaries in polycrystalline naphthalene, J. Phys. Chem. C 117 (2013) 15741.
[49] J.S. Binkley, J.A. Pople, W.J. Hehre, Self-consistent molecular orbital methods. 21. Small split-valence basis sets for first-row elements, J. Am. Chem. Soc. 102 (1980) 939.

[50] W.J. Stevens, H. Basch, M. Krauss, Compact effective potentials and efficient shared-exponent basis sets for the first- and second-row atoms, J. Chem. Phys. 81 (1984) 6026.
[51] K.L. Schuchardt, B.T. Didier, T. Elsethagen, L. Sun, V. Gurumoorthi, J. Chase, J. Li, T.L. Windus, Basis set exchange: a community database for computational sciences, J. Chem. Inf. Model. 47 (2007) 1045.
[52] D. Feller, The role of databases in support of computational chemistry calculations, J. Comput. Chem. 17 (1996) 1571.
[53] N. Godbout, D.R. Salahub, J. Andzelm, E. Wimmer, Optimization of Gaussian-type basis sets for local spin density functional calculations. Part I. Boron through neon, optimization technique and validation, Can. J. Chem. 70 (1992) 560.
[54] Ž. Bodroški, N. Vukmirović, S. Škrbić, Towards the High Performance Method for Large-Scale Electronic Structure Calculations, Springer International Publishing, 2016, p. 90.
[55] T. Petersson, B. Hellsing, A detailed derivation of gaussian orbital-based matrix elements in electron structure calculations, Eur. J. Phys. 31 (2010) 37.
[56] L.E. McMurchie, E.R. Davidson, Calculation of integrals over ab initio pseudopotentials, J. Comput. Phys. 44 (1981) 289.
[57] P.M.W. Gill, Molecular integrals over Gaussian basis functions, Adv. Quantum Chem. 25 (1994) 141.
[58] M. Head-Gordon, J.A. Pople, A method for two-electron Gaussian integral and integral derivative evaluation using recurrence relations, J. Chem. Phys. 89 (1988) 5777.
[59] C.A. White, B.G. Johnson, P.M. Gill, M. Head-Gordon, The continuous fast multipole method, Chem. Phys. Lett. 230 (1994) 8.
[60] E. Rudberg, P. Salek, Efficient implementation of the fast multipole method, J. Chem. Phys. 125 (2006) 084106.
[61] E.A. Toivanen, S.A. Losilla, D. Sundholm, The grid-based fast multipole method – a massively parallel numerical scheme for calculating two-electron interaction energies, Phys. Chem. Chem. Phys. 17 (2015) 31480.
[62] L. Füsti-Molnár, P. Pulay, The Fourier transform Coulomb method: efficient and accurate calculation of the Coulomb operator in a Gaussian basis, J. Chem. Phys. 117 (2002) 7827.
[63] L. Genovese, A. Neelov, S. Goedecker, T. Deutsch, S.A. Ghasemi, A. Willand, D. Caliste, O. Zilberberg, M. Rayson, A. Bergman, R. Schneider, Daubechies wavelets as a basis set for density functional pseudopotential calculations, J. Chem. Phys. 129 (2008) 014109.
[64] O. Treutler, R. Ahlrichs, Efficient molecular numerical integration schemes, J. Chem. Phys. 102 (1995) 346.
[65] A.D. Becke, A multicenter numerical integration scheme for polyatomic molecules, J. Chem. Phys. 88 (1988) 2547.
[66] V. Lebedev, Values of the nodes and weights of ninth to seventeenth order Gauss–Markov quadrature formulae invariant under the octahedron group with inversion, USSR Comput. Math. Math. Phys. 15 (1975) 44.
[67] LAPACK, http://www.netlib.org/lapack, last accessed 4 April 2018.

Supplementary Material: Gaussian Basis Implementation of the Charge Patching Method

Zarko Bodroski[a], Nenad Vukmirović[b,**], Srdjan Skrbic[a,*]

[a] *University of Novi Sad, Faculty of Sciences, Department of Mathematics and Informatics, Trg Dositeja Obradovica 4, 21000 Novi Sad, Serbia*
[b] *Scientific Computing Laboratory, Center for the Study of Complex Systems, Institute of Physics Belgrade, University of Belgrade, Pregrevica 118, 11080 Belgrade, Serbia*

*Corresponding author
**Principal corresponding author
Email addresses: zarko.bodroski@dmi.uns.ac.rs (Zarko Bodroski), nenad.vukmirovic@ipb.ac.rs (Nenad Vukmirović), srdjan.skrbic@dmi.uns.ac.rs (Srdjan Skrbic)

system	atom types	motifs	system for motif generation
alkane oligomers	C_2, C_3, H	C_3-C_2HHH, $C_2-C_3C_2HH$, $C_2-C_2C_2HH$, $H-C_3-C_2HH$, $H-C_2-C_3C_2H$, $H-C_2-C_2C_2H$	$C_{10}H_{22}$
silicon nanocrystals	Si, H	$Si-SiSiSiSi$, $Si-SiSiSiH$, $Si-SiSiHH$, $H-Si-SiSiSi$, $H-Si-SiSiH$	$Si_{29}H_{36}$
boron nitride nanoflakes	B_1, B_2, H N_1, N_2	$B_1-N_1N_1N_1$, $B_1-N_2N_1N_1$, $B_1-N_2N_2N_1$, $B_2-N_1N_1H$, $B_2-N_2N_1H$, $B_2-N_2N_2H$, $H-B_2-N_1N_1$, $H-B_2-N_2N_1$, $H-B_2-N_2N_2$, $H-N_2-B_1B_1$, $H-N_2-B_2B_1$, $H-N_2-B_2B_2$, $N_1-B_1B_1B_1$, $N_1-B_2B_1B_1$, $N_1-B_2B_2B_1$, $N_2-B_1B_1H$, $N_2-B_2B_1H$, $N_2-B_2B_2H$	$B_{19}N_{19}H_{16}$
thiophene oligomers	C_2, C_3, C_4, H, S	$C_2-C_3C_2H$, $C_3-C_3C_2S$, $C_2-C_4C_2H$, C_4-C_2SH, $S-C_3C_3$, $S-C_4C_3$, $H-C_2-C_3C_2$, $H-C_2-C_4C_2$, $H-C_4-C_2S$	$C_{12}S_3H_8$
furane oligomers	C_2, C_3, C_4, H, O	$C_2-C_3C_2H$, $C_3-C_3C_2O$, $C_2-C_4C_2H$, C_4-C_2OH, $O-C_3C_3$, $O-C_4C_3$, $H-C_2-C_3C_2$, $H-C_2-C_4C_2$, $H-C_4-C_2S$	$C_{12}O_3H_8$
halide substituted thiophenes (X=Cl or F)	C_2, C_3, C_4, H, S, X	$C_2-C_3C_2H$, $C_3-C_3C_2S$, $C_2-C_4C_2X$, C_4-C_2SH, $S-C_3C_3$, $S-C_4C_3$, $H-C_2-C_3C_2$, $X-C_2-C_4C_2$, $X-C_2-C_3C_2$, $H-C_4-C_2S$, $C_2-C_3C_2X$	$C_{12}S_3X_3H_5$
disordered P3HT	C_2, C_3, C_4, C_5, C_6, C_7, H, S	$C_5-C_6C_4C_2$, $C_2-C_5C_3H$, $C_3-C_3C_2S$, C_4-C_5SH, $C_3-C_5C_3S$, $C_5-C_6C_3C_2$, C_4-C_2SH, $C_2-C_5C_4H$, $S-C_3C_3$, $S-C_4C_3$, $C_6-C_6C_5HH$, $C_6-C_6C_6HH$, C_7-C_6HHH, $C_6-C_7C_6HH$, $H-C_2-C_5C_3$, $H-C_4-C_5S$, $H-C_2-C_5C_4$, $H-C_4-C_2S$, $H-C_6-C_6C_5H$, $H-C_6-C_6C_6H$, $H-C_7-C_6HH$, $H-C_6-C_7C_6H$	77-atom disordered P3HT

Table 1: The list of atom types and motifs used for charge patching. A certain type is assigned to an atom in a way indicated in Fig. 1.

system	$C_{10}H_{22}$	$C_{20}H_{42}$	$C_{40}H_{82}$
$\delta\varepsilon$ (mHa)	1.6	1.7	1.7
system	$Si_{29}H_{36}$	$Si_{59}H_{60}$	$Si_{87}H_{76}$
$\delta\varepsilon$ (mHa)	3.4	3.1	3.3
system	$C_{12}S_3H_8$	$(C_{12}S_3H_8)_3$	$(C_{16}S_4H_{10})_4$
$\delta\varepsilon$ (mHa)	2.1	2.1	2.0

Table 2: Mean square difference $\delta\varepsilon = \sqrt{\left\langle (\Delta\varepsilon)^2 \right\rangle}$ of occupied state eigenenergies obtained using Gaussian basis CPM code and plane wave basis CPM code.

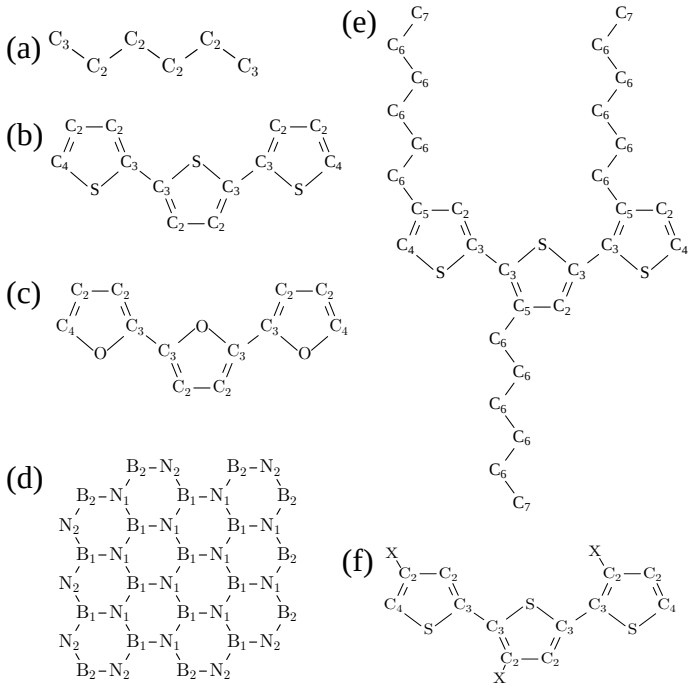

Figure 1: Atomic type classification in the case of: (a) alkanes oligomers; (b) thiophene oligomers; (c) furane oligomers; (d) boron-nitride nanoflakes; (e) P3HT; (f) halide-substituted thiophene oligomers.

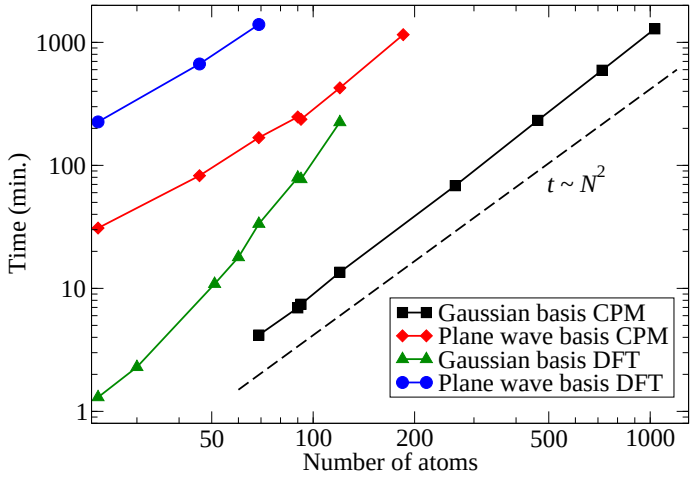

Figure 2: Comparison of the dependence of computational time on the number of atoms in the case of a two-dimensional array of polythiophene chains for Gaussian basis and plane wave basis DFT and CPM codes. The dashed line showing $t \sim N^2$ dependence is given as a guide to the eye.

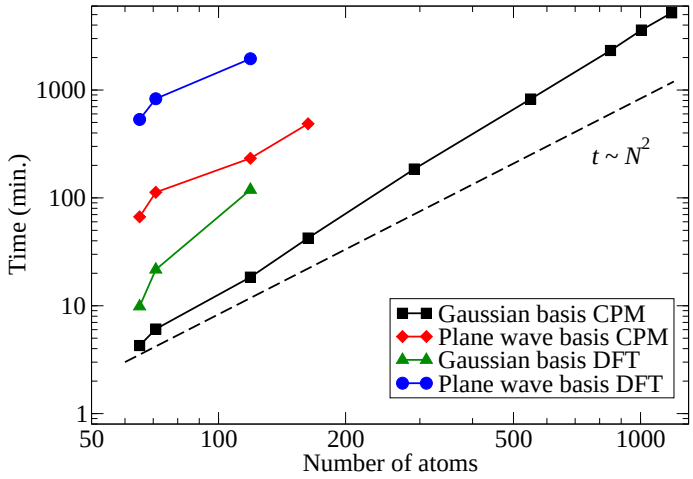

Figure 3: Comparison of the dependence of computational time on the number of atoms in silicon nanocrystals for Gaussian basis and plane wave basis DFT and CPM codes. The dashed line showing $t \sim N^2$ dependence is given as a guide to the eye.